UMYU Scientifica, Vol. 5 NO. 2, June 2026, Pp 241 – 255
https://doi.org/10.56919/usci.2652.023
ISSN: 2955 – 1145 (print); 2955 – 1153 (online)
A periodical of the Faculty of Natural and Applied Sciences, UMYU, Katsina

ORIGINAL RESEARCH ARTICLE

Synthesis and Computational Evaluation of PET-based Polymer Composites for the Adsorption of Chlorophenol

Hitler Louis*[1,2], Theresa O. Egbuchunam[1], Vivian K. Orisakwe[1] and Idongesit J. Mbonu[1]
[1]Department of Chemistry, College of Science, Federal University of Petroleum Resources, Effurun, Nigeria
[2]Department of Pure and Applied Chemistry, University of Calabar, Calabar, Nigeria

ABSTRACT
In this study, a combined experimental and theoretical approach was employed to evaluate the adsorption performance of polyethylene terephthalate (PET), polyurethane (PU), and TiO_2-doped PET/PU microplastics for the remediation of *para*-chlorophenol (PCP), a petroleum phenolic pollutant. PET and PU microplastics were synthesized via carbonation and sieving techniques, while the nanocomposite was obtained through low-temperature calcination of PET, PU, and TiO_2 in equal proportions. The FT-IR analyses provided insight into the structural and morphological characterization, confirming the successful fabrication of the composite. Density functional theory (DFT) calculations, using the B3LYP-D3/Def2SVP method, provided insights into the electronic behavior and adsorption mechanisms. The TiO_2-PET/PU nanocomposite exhibited a reduced energy gap of 2.489 eV and the highest chemical potential (μ) of −4.527 eV among the studied systems, indicating improved reactivity and charge transfer capability. Upon PCP adsorption, the composite exhibited a significantly enhanced electrophilicity index (ω) of 8.234 eV, along with the most favorable adsorption energy (E_{ads} = −2.594 eV), which were carried out computationally, surpassing both pristine PET (−0.629 eV) and PU (−0.656 eV), respectively. These findings demonstrate that TiO_2-functionalized PET/PU microplastics hold strong promise as efficient sorbents for chlorophenol removal in environmental applications.

ARTICLE HISTORY
Received January 05, 2026
Accepted June 14, 2026
Published June 16, 2026

KEYWORDS
PET/PU microplastics, composites, adsorption, chlorophenol

INTRODUCTION
The persistence of petroleum-derived pollutants in aquatic environments poses a significant challenge to global water security and environmental sustainability (Watkins et al., 2017). Chlorophenols are classified as ecological hormones (EHs), recognized for their carcinogenicity, acute toxicity, and role as precursors to highly persistent dioxins (Mathew et al., 2025; Beigh, 2024). In recent years, increasing attention has been devoted to their removal from the environment, making this a prominent research hotspot and rendering them priority pollutants (Wei et al., 2019). Therefore, the development of cost-effective and sustainable remediation strategies for chlorophenol removal is of both scientific and environmental importance.

Microplastics, typically regarded as environmental threats, especially in aquatic systems, are increasingly being reconsidered as functional sorbents owing to their high surface area, tunable surface chemistry, and stability under harsh environmental conditions (Zhao et al., 2024; Das et al., 2024; Alkhaldi et al., 2024). Polyethylene terephthalate (PET) and polyurethane (PU) are among the most abundant microplastic residues generated from consumer products, industrial packaging, and coatings (Shi et al., 2023; An et al., 2020). Their structural motifs, aromatic rings, carbonyl groups, and urethane functionalities offer multiple potential binding sites for hydrophobic, π–π, hydrogen bonding, and electrostatic interactions with chlorophenol species (An et al., 2020; VL et al., 2025; Cova et al., 2021; Liu et al., 2021). Harnessing these intrinsic features transforms a problematic pollutant (microplastics) into a resource for pollutant remediation, thereby advancing circular and sustainable approaches to environmental management.

Despite this promise, understanding how chlorophenols adsorb on PET/PU-based microplastics remains limited. Previous studies conducted by Jiang & Hu (2024) showed that microplastics (MPs) acted as carriers for tetracycline (TC) in water, and enhanced adsorption when combined with vitamin C-modified crayfish shell biochar (CSB-VC). Aged polyethylene, polypropylene, and polyvinyl chloride exhibited high capacities (275–285 mg/g) and maintained >245 mg/g in real water systems. A study by Liu et al. (2020) used polyethylene terephthalate (PET, <150 μm) as the adsorbent and chlorophenols (MCP, DCP, TCP) as

Correspondence: Hitler Louis. Department of Chemistry, College of Science, Federal University of Petroleum Resources, Effurun, Nigeria. ✉ louismuzong@gmail.com.
How to cite: Louis, H., Egbuchunam, T. O., Orisakwe, V. K., & Mbonu, I. J. (2026). Synthesis and Computational Evaluation of PET-based Polymer Composites for the Adsorption of Chlorophenol. *UMYU Scientifica*, 5(2), 241 – 255. https://doi.org/10.56919/usci.2652.023

model pollutants. Results showed that while ionic strength, fulvic acid, and natural water matrices reduced the adsorption of DCP and TCP, the adsorption of MCP remained stable across conditions, with consistent Kd values (≈10.6–11.4 L/kg). The overall adsorption affinity followed the order DCP > MCP > TCP. In another study by Enyoh & Wang (2024), the adsorption of phenol onto pristine (Pr-PET), modified (Mod-PET), and aged (Ag-PET) PET microplastics was investigated using both experimental and theoretical approaches. Their findings showed that among the tested systems, Ag-PET showed the highest removal efficiency due to its larger surface area, while the maximum adsorption capacity followed the order Mod-PET (38.02 mg/g) > Ag-PET (8.08 mg/g) > Pr-PET (6.84 mg/g). Bio-Graphene Foams (BGFs) were innovatively synthesized from sustainable resources using a two-step method, yielding a highly porous structure with a surface area of 805 m^2/g by Sidra et al. (2024). The BGFs exhibited exceptional adsorption performance for 2,4-dichlorophenol (DCP) and 2,4,6-trichlorophenol (TCP), achieving a maximum capacity of 245 mg/g at pH 3–4, consistent with the Langmuir isotherm (Frescura et al., 2024; Jiang et al., 2022; Costa et al., 2024). Theoretical simulations, like density functional theory (DFT) combined with electronic structure analysis, complement experiments by calculating adsorption energies, identifying interaction regions, and revealing charge transfer pathways.

In this study, we address the limited understanding of how blended PET-based microplastics engineered with metal oxide functionalities influence chlorophenol adsorption. While previous studies have examined PET or other polymeric sorbents individually, systematic investigation of PET/PU blended microplastics integrated with TiO_2 and supported by molecular-level computational analysis remains scarce. Here, we combine experimental synthesis and density functional theory (DFT) modeling to clarify both adsorption performance and mechanism. Experimentally, PET and PU microplastics were prepared via carbonation and sieving processes, followed by the formation of PET/PU–TiO_2 composites through low-temperature calcination at controlled equal proportions, a condition selected to promote interfacial dispersion of TiO_2 and the generation of heterogeneous adsorption sites. We hypothesize that the PET/PU blend provides complementary functional environments, aromatic domains from PET, and polar urethane groups from PU, while TiO_2 incorporation enhances surface polarity, charge distribution, and potential hydrogen-bonding or donor-acceptor interactions with chlorophenol. To test this hypothesis and rationalize adsorption behavior, DFT calculations at the B3LYP-D3/Def2SVP level were employed to evaluate adsorption energies, frontier molecular orbitals (FMO), natural bond orbital (NBO) charge transfer, molecular electrostatic potential (MESP), and non-covalent interaction (NCI) characteristics. Thus, the objective of this work is twofold: (i) to experimentally validate PET/PU–TiO_2 composites as effective sorbents for chlorophenol removal, and (ii) to use computational analysis to predict adsorption trends and elucidate the underlying interaction mechanisms that govern sorption performance. This integrated approach establishes a mechanistic basis for designing PET-derived polymer composites with improved adsorption capability for water treatment applications.

METHODS

2.1 Experimental

2.1.1 Preparation of PET microplastics

Empty PET bottles were collected, washed thoroughly with distilled water to remove surface contaminants, and air-dried. The bottles were cut into smaller pieces manually to reduce their size before processing. The PET fragments were placed in a porcelain crucible and subjected to controlled thermal softening over a Bunsen burner for a short duration (approximately 2–3 min) to allow melting without prolonged combustion. The molten material was allowed to cool at room temperature and subsequently mechanically ground using a laboratory mortar grinder to obtain smaller particles. The ground material was sieved using a 200-mesh sieve (≈75 μm particle size) to obtain PET microplastic powder. To ensure that the polymer backbone remained intact after thermal treatment, structural integrity was verified using FTIR analysis as described in Section 2.2.

2.1.2 Preparation of PU microplastics

Polyurethane (PU) foam was cut into smaller pieces and cleaned to remove dust and impurities. The material was then placed in a crucible and thermally treated under limited exposure to direct flame in an aerated environment for a short period to reduce the bulk material into brittle fragments rather than complete combustion. The obtained material was allowed to cool at room temperature and subsequently ground to produce fine particles. The powdered sample was sieved using a 200-mesh sieve (~75 μm) to obtain PU microplastic powder. The chemical structure of PU after processing was confirmed by FTIR spectroscopy to verify the presence of characteristic urethane functional groups.

2.1.3 Synthesis of TiO_2-doped PET/PU nanocomposite

A blend ratio of PET: PU = 1:1 (w/w) was used for composite preparation. Specifically, 2 g of PET powder and 2 g of PU powder were weighed and mixed. Commercial TiO_2 nanoparticles (added at an equal mass proportion relative to the polymer mixture; TiO_2 loading ≈ 50 wt%) were introduced into the mixture. The components were dispersed in 50 mL of distilled water and stirred using a magnetic stirrer at 500 rpm for 2h at room temperature (≈25 °C) to ensure uniform mixing. The pH of the suspension was maintained at approximately neutral (pH ≈ 7) during mixing. After mixing, the sample was transferred into an oven and thermally treated at 100 °C for 12 h to remove moisture and promote composite stabilization. This step is referred to as low-temperature thermal treatment/drying rather than calcination, since calcination typically occurs at temperatures above 400 °C. The dried composite was then

ground using a mortar and pestle and sieved again through a 200-mesh sieve (~75 µm) to obtain a homogeneous TiO_2-doped PET/PU composite powder. The reaction procedure is illustrated in Scheme 1.

2.2 Characterization of TiO_2-doped PET/PU nanocomposite

The structural properties of the synthesized composite were analyzed using X-ray diffraction (XRD). Measurements were performed using Cu Kα radiation (λ = 1.541 Å) operated at 40 kV and 30 mA, with a scanning range of 2θ = 10–80° and a scan rate of 2° min^{-1}. Fourier transform infrared (FTIR) spectroscopy was carried out to identify functional groups and confirm polymer integrity after processing. Spectra were recorded in the range of 400–4000 cm^{-1} using the KBr pellet method. In addition, particle size distribution of the prepared microplastics was controlled through sieving (~75 µm), and the dispersion of TiO_2 within the polymer matrix was evaluated from XRD peak characteristics and FTIR spectral features.

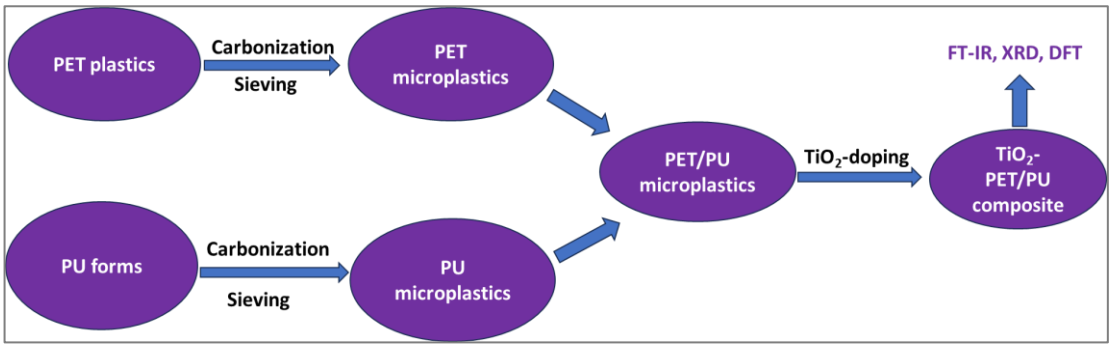

Scheme 1: The schematic design of the composite reaction procedures.

2.3 Theoretical calculation method

The present computational studies on the designed surfaces (PET, PU, and TiO_2-PET/PU) and chlorophenol (PCP) adsorbed complexes were carried out using the Gaussian 16 program package (Frisch et al., 2016) within the framework of Density Functional Theory (DFT) to evaluate their structural, electronic, and reactive properties. Geometry optimizations were performed at the B3LYP-D3/Def2-SVP level of computation while maintaining minimum ground energy; the surfaces were stabilized at a singlet multiplicity with a net charge of zero (Semenov et al., 2023). The B3LYP hybrid exchange–correlation functional, which combines Becke's three-parameter exchange with the Lee-Yang-Parr correlation (Becke, 1993), was adopted due to its proven accuracy in predicting molecular geometries, frontier orbital energies, and intermolecular interactions (Huang et al., 2017; Guan et al., 2025). The Def2SVP basis set was employed to balance computational efficiency and accuracy and offers better treatment of transition metals and heavier main-group elements, while still being less computationally demanding than larger triple-ζ sets (Goodfellow & Bühl, 2021; Semidalas & Martin, 2020; Bytautas et al., 2022). PET and PU were represented by oligomeric fragments to capture the relevant functional groups involved in adsorption, while TiO_2 was modeled using a finite cluster representing the active adsorption surface. All structures were fully optimized without symmetry constraints. Adsorption energies were calculated using:

$$E_{ads} = E_{complex} - (E_{adsorbent} + E_{PCP}) \quad (1)$$

where $E_{complex}$ represents the total energy of the adsorption system, and $E_{adsorbent}$ and E_{PCP} correspond to the energies of the isolated sorbent and chlorophenol molecule, respectively. Frequency calculations were performed to verify that optimized geometries correspond to true minima on the potential energy surface. Gas-phase calculations were employed to evaluate relative adsorption trends and interaction mechanisms between the sorbent and chlorophenol molecules. Default Gaussian convergence criteria and integration grids were used during all calculations.

The frontier molecular orbitals (HOMO-LUMO plots) were visualized using the Chemcraft software program (Zhurko & Zhurko, 2005), based on the formatted checkpoint files derived from optimized geometries. Natural bond orbital (NBO) analysis gives insight into the electronic perturbation between donor and acceptor molecular orbitals of the systems (Weinhold, 2012). Furthermore, the Molecular Electrostatic Potential (MESP), Quantum Theory of Atoms in Molecules (QTAIM) topological analysis (Table 3), and Non-Covalent Interaction (NCI) plots were generated using the Multiwfn 3.7 software package (Lu & Chen, 2012) and visualized with Visual Molecular Dynamics (VMD) 1.9.3 (Humphrey et al., 1996). These analyses provided critical insights into the electrophilic and nucleophilic regions, bonding characteristics, and weak non-covalent interactions present in the studied systems, which are essential for understanding their adsorption and catalytic behaviors.

RESULTS AND DISCUSSION

3.1 Materials Characterization

3.1.1 FT-IR

Fourier-transform infrared (FT-IR) spectroscopy is a powerful tool for probing the surface chemistry and molecular structure of polymers and their composites. It provides direct evidence of functional groups present, their bonding environments, and possible modifications upon blending or incorporation of additives (Mohamed et al., 2017; Combrzyński et al., 2021; Ali et al., 2021). In the present study, FTIR was employed to confirm the

structural features of PET, PU, and the PU-PET-TiO_2 composite, identify functional groups that may participate in pollutant binding, and evaluate chemical interactions introduced by TiO_2 incorporation.

The combined FT-IR spectra of PET, PU, and PU-PET-TiO_2 composites are presented in Figure 1. For PET, the characteristic absorption peaks were observed at 1712 cm^{-1}, corresponding to the C=O stretching vibration of ester groups (Kumar et al., 2019), along with bands at 1239-1100 cm^{-1} attributed to C-O-C stretching (Yusuf, 2023; Mecozzi & Nisini, 2019), 1239, 1339, and 1407cm^{-1} (C-H stretching) and ~2965–2907 cm^{-1} assigned to aliphatic C-H stretching. We also observe bands at 1015, 971, 898, 870, 846, 792, and 721cm^{-1}, which correspond to C-H stretching (Kumar et al., 2019; Markandan et al., 2020). In the case of PU, distinctive peaks appeared at 2868, 2928, 2969, and 3026 cm^{-1}, which are attributed to both asymmetric and symmetric stretching vibrations. 1718 cm^{-1} corresponds to urethane C=O stretching (Yi et al., 2020). 1600–1450 cm^{-1} depicts the amide II band due to N-H bending and C-N stretching, and ~1090 cm^{-1} C-N stretching of the urethane linkage.

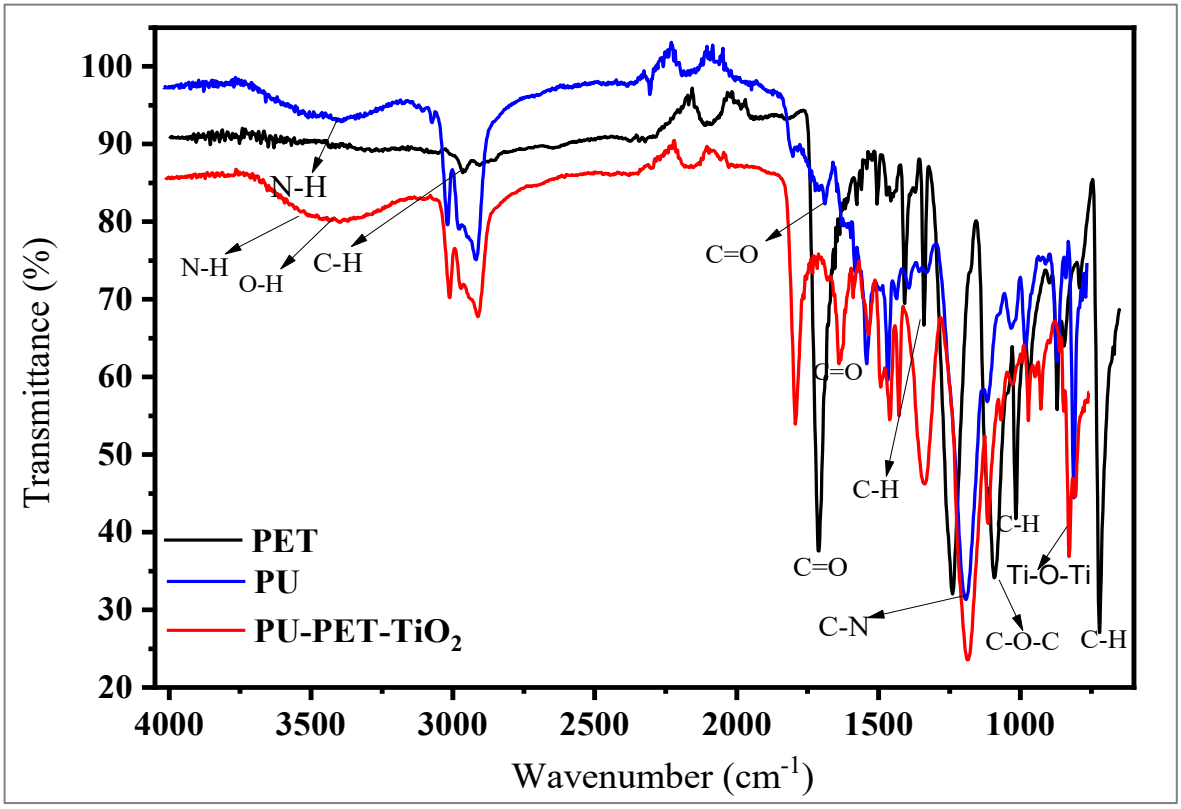

Figure 1. FTIR spectra of PET, PU, and PU-PET-TiO_2 composites

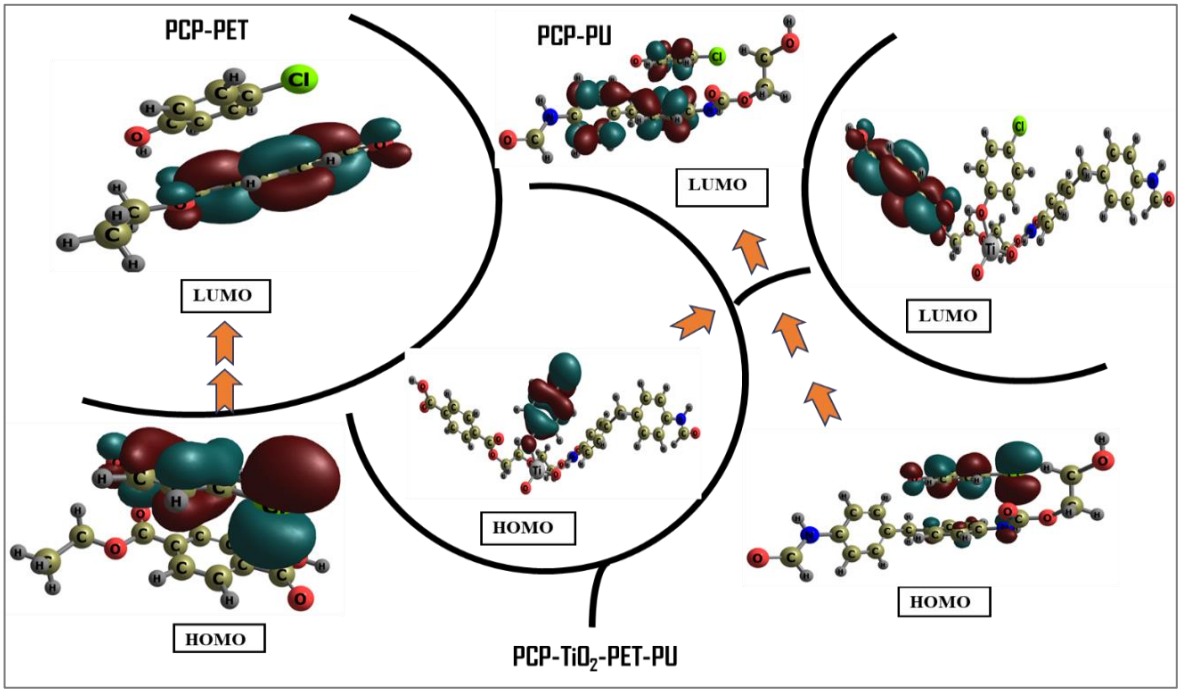

Figure 2. The HOMO-LUMO distribution maps of PCP-PET, PCP-PU, and PCP-TiO_2-PET-PU complexes.

The spectrum of the PU-PET-TiO_2 composite exhibited notable changes compared to pristine PET and PU. A broadening and slight shift of the O-H/N-H stretching band (~3300 cm^{-1}) was observed, indicating hydrogen bonding interactions between polymeric functional groups and surface hydroxyls of TiO_2. Furthermore, enhanced absorption in the 1000-600 cm^{-1} region can be ascribed to Ti-O-Ti vibrations, confirming the successful incorporation of TiO_2 (Adak et al., 2019).

Table 1. Energies of HOMO (eV), LUMO (eV), HOMO-LUMO energy gap (Egap) (eV), Chemical Softness (σ, eV), hardness (η, eV), chemical potential (μ, eV), and electrophilicity index (ω, eV) calculated using the DFT/B3LYP/Def2SVP-D3 level of theory.

SYSTEMS	HOMO/eV	LUMO/eV	Energy gap	σ(eV)	η(eV)	μ(eV)	ω(eV)	E_{ads}(eV)
PET	-7.458	-2.156	5.302	0.189	2.651	-4.807	4.358	-
PU	-6.007	-0.729	5.278	0.189	2.639	-3.368	2.149	-
TiO_2-PET-PU	-5.834	-2.675	3.16	0.317	1.58	-4.254	5.729	-
PCP-PET	-6.199	-2.175	4.024	0.249	2.012	-4.187	4.357	-0.629
PCP-PU	-5.944	-0.771	5.173	0.193	2.587	-3.357	2.179	-0.656
PCP-TiO_2-PET-PU	-5.772	-3.283	2.489	0.402	1.245	-4.527	8.234	-2.594

Table 2. The calculated NBO Donor (i), Acceptor (j), and second-order perturbation-stabilization energies ($E^{(2)}$ kcal/mol) of the complexes

SYSTEM	Donor (i)	Occupancy	Acceptor (j)	Occupancy	$E^{(2)}$ (kcal/mol)	E(j)-E(i) a.u	F(i,j) a.u
PET	π^*C_{14} - O_{15}	0.25338	π^*C_4 - C_5	0.35536	135.22	0.02	0.074
	π^*C_{11} - O_{12}	0.24833	π^* C_1 - C_6	0.36532	126.02	0.02	0.073
PU	π^*C_{19} - C_{21}	0.401	π^*C_{14} - C_{16}	0.36042	232.49	0.01	0.082
	π^*C_{19} - C_{21}	0.401	π^*C_{15} - C_{17}	0.31272	192.38	0.02	0.083
TiO_2-PET-PU	π^*C_{19} - C_{21}	0.38916	π^*C_{15} - C_{17}	0.32144	284.99	0.01	0.083
	π^*C_9 - C_{11}	0.39587	π^*C_4 - C_6	0.35056	221.99	0.01	0.083
PCP-PET	π^*C_{29} - C_{30}	0.40275	π^*C_{25} - C_{26}	0.3362	259.36	0.01	0.081
	π^*C_{11} - O_{12}	0.2462	π^*C_1 - C_2	0.35302	128.09	0.02	0.074
PCP-PU	π^*C_7 - C_{11}	0.39959	π^*C_4 - C_5	0.35223	226.36	0.01	0.083
	π^*C_{44} - C_{45}	0.3972	π^*C_{42} - C_{43}	0.31273	200.04	0.02	0.084
PCP-TiO_2-PET-PU	$LP_{(3)}$ O_{77}	1.60557	$LP^*_{(1)}$ H_{78}	0.44943	392.35	0.67	0.464
	π^*C_9 - C_{11}	0.39585	π^*C_4 - C_6	0.35147	226.8	0.01	0.083

Table 3: The calculated topological parameters

SYSTEMSw	Bonds	CP	$\varrho_{(r)}$	$\nabla^2\varrho^{(r)}$	$G_{(r)}$	$K_{(r)}$	$V_{(r)}$	$H_{(r)}$	$G_{(r)}/V_{(r)}$	ELF	ε	λ_1	λ_2	λ_3
PCP-PET	$O_{35} - H_{20}$	75	0.008	0.037	0.007	-0.002	-0.005	0.002	-1.4	0.02	0.127	-0.009	-0.008	0.055
	$Cl_{37} - C_2$	69	0.005	0.017	0.003	-0.001	-0.003	0.001	-1	0.017	0.407	-0.002	-0.002	0.021
	$O_{15} - H_{36}$	63	0.014	0.062	0.013	-0.003	-0.01	0.003	-1.3	0.03	0.113	-0.017	-0.015	0.093
	$C_{28} - C_4$	61	0.006	0.023	0.004	-0.002	-0.003	0.002	-1.333	0.016	1.9	-0.003	-0.001	0.027
PCP-PU	$Cl_{54} - C_{35}$	78	0.005	0.018	0.004	-0.001	-0.003	0.001	-1.333	0.013	3.539	-0.003	-0.001	0.022
	$Cl_{54} - N_{29}$	82	0.006	0.02	0.004	-0.001	-0.003	0.001	-1.333	0.02	2.059	-0.004	-0.001	0.025
	$O_{32} - H_{22}$	63	0.011	0.054	0.01	-0.003	-0.007	0.003	-1.429	0.023	0.613	-0.011	-0.007	0.072
	$O_{32} - H_{48}$	76	0.007	0.03	0.006	-0.002	-0.004	0.002	-1.5	0.015	0.052	-0.007	-0.007	0.043
	$O_{52} - H_{10}$	123	0.008	0.039	0.007	-0.002	-0.005	0.002	-1.4	0.018	0.11	-0.01	-0.009	0.058
	$O_{52} - H_2$	124	0.005	0.019	0.004	-0.001	-0.002	0.001	-2	0.011	0.166	-0.004	-0.004	0.027
	$C_{43} - C_{15}$	101	0.004	0.018	0.003	-0.001	-0.002	0.001	-1.5	0.012	10.054	-0.003	0	0.02
PCP-TiO_2-PET-PU	$O_{55} - H_{75}$	105	0.006	0.028	0.005	-0.002	-0.003	0.002	-1.667	0.011	0.623	-0.006	-0.003	0.037
	$O_{55} - H_{78}$	125	0.045	0.162	0.042	0.001	-0.043	-0.001	-0.977	0.134	0.005	-0.087	-0.086	0.335
	$O_{65} - H_{74}$	154	0.008	0.32	0.006	-0.002	-0.004	0.002	-1.5	0.022	0.193	-0.007	-0.006	0.046
	$C_{19} - H_{74}$	142	0.008	0.032	0.006	-0.002	-0.004	0.002	-1.5	0.02	0.206	-0.007	-0.006	0.045
	$O_{32} - H_{22}$	151	0.015	0.075	-0.004	-0.011	0.004	0.075	-1	0.032	0.229	-0.018	-0.015	0.107
	$C_{17} - H_{73}$	116	0.005	0.021	0.004	-0.002	-0.002	0.002	-2	0.011	2.088	-0.004	-0.001	0.026
	$C_{68} - H_{38}$	137	0.003	0.011	0.002	-0.001	-0.001	0.001	-2	0.009	0.106	-0.002	-0.002	0.015

Electron density $\varrho(r)$, Laplacian electron density $\nabla^2\varrho(r)$, Lagrangian kinetic energy G(r), Potential electron energy density V(r), Total electron energy density H(r), Eigen values ($\lambda1$, $\lambda2$, $\lambda3$), electron delocalized function (ELF), and Ellipticity (ε) of the studied complexes at the bond critical points (BCPs). All values are in a.u.

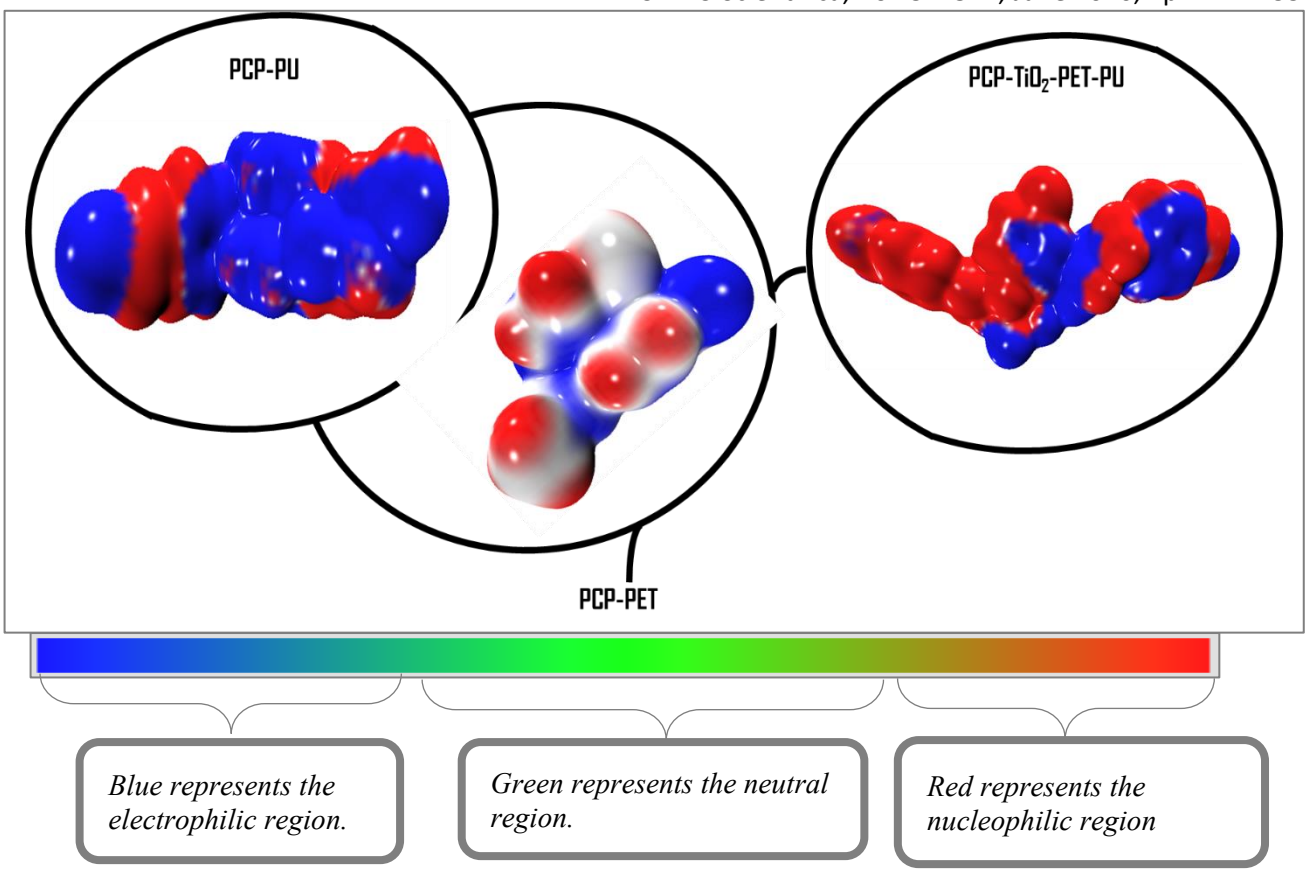

Figure 3. The molecular electrostatic potential (MESP) mapping of the different systems.

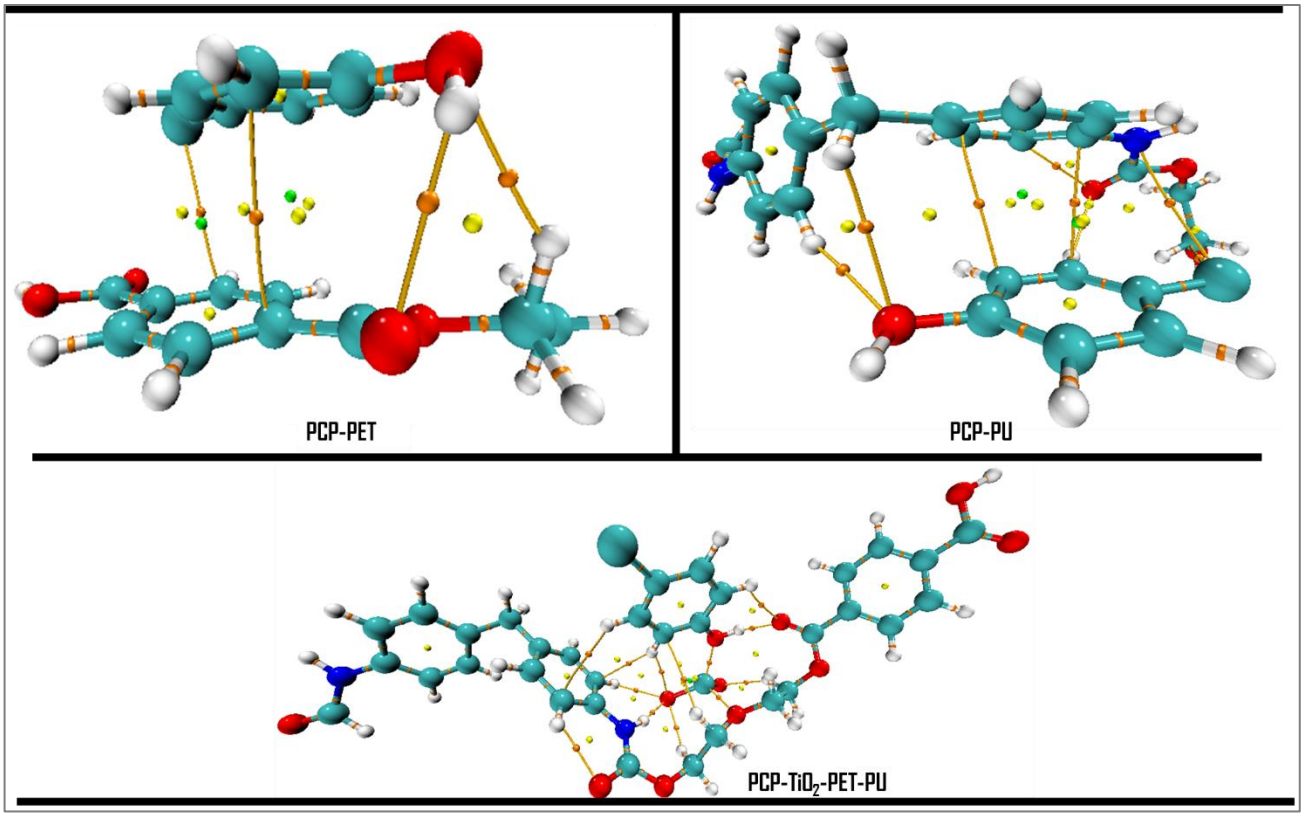

Figure 4. The QTAIM plots of PCP-PET, PCP-PU, and PCP-TiO_2-PET-PU complexes.

Additionally, minor shifts in the C=O stretching band (~1710-1720 cm^{-1}) suggest possible coordination between TiO_2 and the carbonyl groups of PET and PU (Shoukat et al., 2023; Ambrose et al., 2025). Herein, the FTIR results confirm the successful blending of PET and PU, as well as the effective incorporation of TiO_2 into the polymer matrix. The observed structural modifications and newly formed interactions are expected to provide additional adsorption sites, thereby enhancing the composite's affinity toward chlorophenol pollutants.

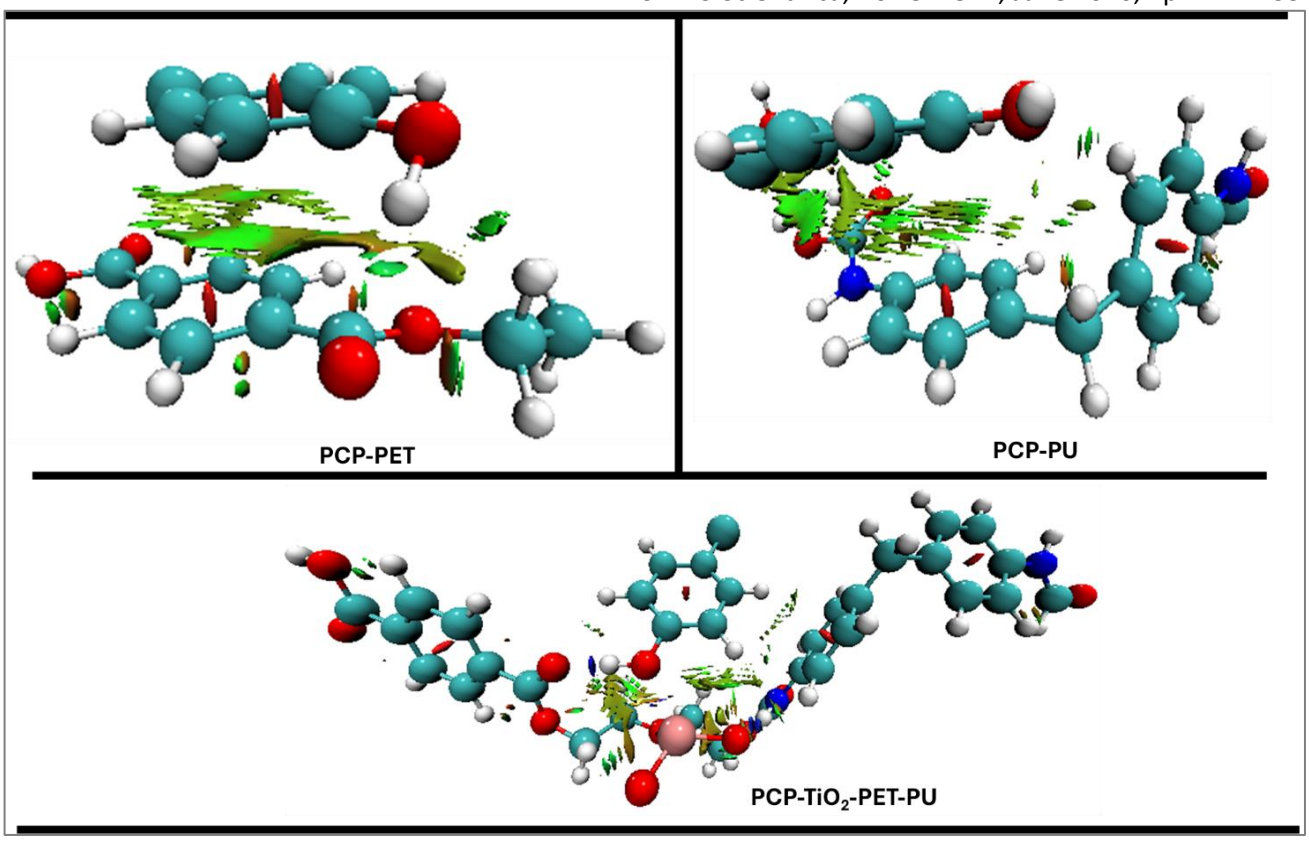

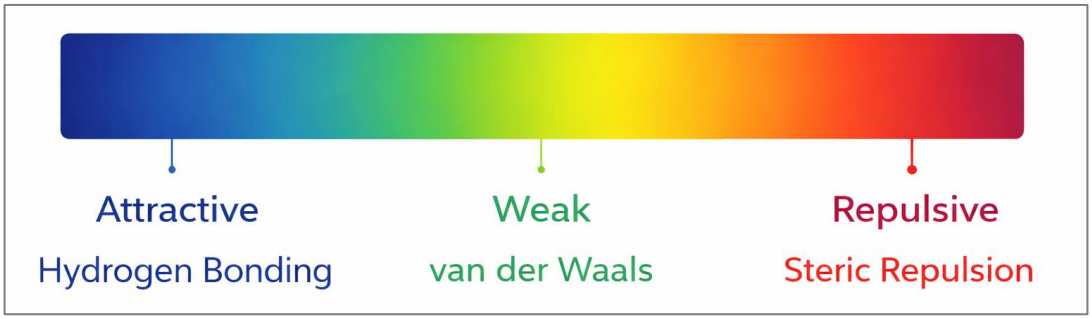

Figure 5: The non-covalent interaction (NCI) plots of PCP-PET, PCP-PU, and PCP-TiO_2-PET-PU complexes

3.2 Electronic properties

3.2.1 HOMO-LUMO studies

Understanding the electronic properties of adsorbent systems is essential for establishing structure–activity relationships in pollutant capture. Frontier molecular orbital energies (HOMO, LUMO) and the derived energy gap (E_{gap}) provide direct insights into the chemical stability and reactivity of the sorbent surface (Cao et al., 2021). Hardness (η) and softness (σ) quantify the polarizability of the material, which governs its ability to adapt electron density during adsorption (Cao et al., 2021; Montazeri et al., 2023). The chemical potential (μ) reflects the electron-donating or -accepting tendency of the system, while the electrophilicity index (ω) measures its capability to stabilize additional electronic charge upon pollutant binding (Khachay et al., 2025), which was calculated by employing equations (1) – (7) (Cao et al., 2021; Montazeri et al., 2023; Khachay et al., 2025). Incorporating these parameters allows a deeper mechanistic understanding of how pristine PET and PU, as well as TiO_2-modified PET/PU composites, interact with chlorophenol molecules beyond experimental adsorption data alone.

$$\mathbf{IP} = -E_{\mathrm{HOMO}} \quad (1)$$

$$\mathbf{EA} = -E_{\mathrm{LUMO}} \quad (2)$$

$$\Delta E = E_{\mathrm{LUMO}} - E_{\mathrm{HOMO}} \quad (3)$$

$$\boldsymbol{\eta} = {}^{1}/_{2}\,(IP - EA) = \frac{E_{\mathrm{LUMO}} - E_{\mathrm{HOMO}}}{2} \quad (4)$$

$$\boldsymbol{\sigma} = \frac{1}{2\eta} = \frac{1}{IP - EA} = \frac{1}{E_{\mathrm{LUMO}} - E_{\mathrm{HOMO}}} \quad (5)$$

$$\boldsymbol{\mu} = -{}^{1}/_{2}\,(E_{\mathrm{HOMO}} + E_{\mathrm{LUMO}}) \quad (6)$$

$$\boldsymbol{\omega} = \frac{\mu^2}{2\eta} \quad (7)$$

The frontier orbital analysis revealed that pristine PET and PU possess wide HOMO–LUMO gaps of 5.302 and 5.278 eV, respectively, consistent with their chemical stability and low reactivity as shown in Table 1. Incorporation of TiO_2 into the PET/PU matrix significantly reduced the gap to 3.160 eV, accompanied by increased softness (σ = 0.317 eV) and decreased hardness (η = 1.580 eV), indicating enhanced polarizability and charge transfer potential. Upon interaction with PCP, both PET and PU

exhibited slight reductions in their energy gaps (4.024 and 5.173 eV, respectively) with moderate electrophilicity indices (ω ≈ 4.3 and 2.2 eV), suggesting weak adsorption. In contrast, PCP adsorption on the TiO_2-PET/PU composite produced the lowest gap (2.489 eV) and the highest softness (σ = 0.402 eV), confirming substantial electronic perturbation. The electrophilicity index increased markedly to 8.234 eV, while the chemical potential stabilized at −4.527 eV, highlighting strong charge transfer between PCP and the composite surface. These demonstrate that TiO_2 functionalization enhances the reactivity of the PET/PU system and provides superior binding affinity toward PCP compared to pristine PET or PU, corroborating the role of the TiO_2-PET/PU nanocomposite as the most efficient adsorbent. The electronic distribution of the orbital map is shown in Figure 2.

3.2.2 Natural Bond Orbital (NBO) Analysis

The NBO second-order perturbation results ($\mathcal{E}^2$ stabilization energies) give deep insight into donor–acceptor interactions and charge delocalization. The second-order perturbation theory as proposed by Weinhold (2012) was employed to probe donor–acceptor interactions within PET, PU, and TiO_2-PET/PU before and after PCP adsorption, calculated using equation 8 (Weinhold, 2012; Zhang et al., 2022a; Zhang et al., 2022b). In pristine PET, strong π → π* delocalization was observed, particularly from $\pi^*C_{14}–O_{15} \rightarrow \pi^*C_4–C_5$ ($\mathcal{E}^2$ = 135.22 kcal/mol) and $\pi^*C_{11}–O_{12} \rightarrow \pi^*C_1–C_6$ ($\mathcal{E}^2$ = 126.02 kcal/mol). These moderate stabilization energies reflect localized conjugation within the aromatic ester backbone (VL et al., 2025). PU displayed more pronounced delocalization, with $\pi C_{19}–C_{21} \rightarrow \pi^*C_{14}–C_{16}$ interactions yielding an $\mathcal{E}^2$ of 232.49 kcal/mol, suggesting greater electronic delocalization across its aromatic units compared to PET. The TiO_2-PET/PU nanocomposite exhibited even stronger charge delocalization, as evidenced by $\pi C_{19}–C_{21} \rightarrow \pi^*C_{15}–C_{17}$ ($\mathcal{E}^2$ = 284.99 kcal/mol), confirming that TiO_2 incorporation enhances orbital overlap and intramolecular stabilization. This improved delocalization is consistent with the reduced energy gap and increased softness observed for the composite.

$$E^{(2)} = \boldsymbol{qi}\frac{(\boldsymbol{Fij})^2}{\boldsymbol{E(i)-E(j)}} \quad (8)$$

Upon adsorption of PCP, PET, and PU displayed enhanced π → π* transitions, such as $\pi C_{29}–C_{30} \rightarrow \pi^*C_{25}–C_{26}$ in PCP-PET ($\mathcal{E}^2$ = 259.36 kcal/mol) and $\pi C_7–C_{11} \rightarrow \pi^*C_4–C_5$ in PCP-PU ($\mathcal{E}^2$ = 226.36 kcal/mol). These values are significantly higher than in their pristine states, indicating that PCP binding induces stronger conjugation and electronic redistribution within the polymer matrices. In comparison, the most striking stabilization occurred in PCP-TiO_2-PET/PU, where a lone-pair to antibonding interaction $LP_{(3)}O_{77} \rightarrow LP^*_{(1)}H_{78}$ displayed an exceptionally high $\mathcal{E}^2$ value of 392.35 kcal/mol, with strong overlap (F(i,j) = 0.464 a.u). This interaction suggests pronounced hydrogen-bond-assisted charge transfer between PCP and the composite surface, far exceeding the stabilization energies observed in pristine PET or PU. This enhanced $\pi \rightarrow \pi$ delocalization and the exceptionally strong LP→LP* charge transfer interaction observed in PCP–TiO_2-PET/PU highlight the pivotal role of electronic redistribution in strengthening pollutant binding (Zhang et al., 2022a; Zhang et al., 2022b). Also, TiO_2 incorporation significantly enhances electronic delocalization and facilitates stronger intermolecular charge transfer with PCP, thereby rationalizing the superior adsorption energy of the composite system (Farokhi et al., 2022; Arif et al., 2024; Lazić & Nedeljković, 2024). Table 2 shows the calculated NBO Donor (i), Acceptor (j), and second-order perturbation-stabilization energies (E(2) kcal/mol) of the complexes, before and after adsorption of PCP calculated at the DFT/B3LYP-D3/Def2SVP level of theory.

3.2.3 Molecular Electrostatic Potential (MESP)

The MESP plots of PCP-PET, PCP-PU, and PCP-TiO_2-PET/PU (Figure 3) provide insight into the charge distribution and reactive sites of the studied systems. The color-coded surfaces represent electrostatic potential regions, where red corresponds to electron-rich zones (negative potential, nucleophilic sites), while blue indicates electron-deficient zones (positive potential, electrophilic sites) (Suresh & Haritha, 2024; Haritha & Suresh, 2024). For PCP-PET, the surface exhibits a balanced distribution of red and blue regions, reflecting the presence of both electron-rich oxygen functionalities and electron-deficient carbon centers. This distribution indicates moderate polarity, with localized regions that could participate in hydrogen bonding and weak electrostatic interactions.

The PCP-PU system shows an increased concentration of blue regions, suggesting stronger electron-deficient sites. This indicates enhanced electrophilicity, which could promote stronger interactions with nucleophilic species in the environment (Suresh et al., 2022). The extended conjugated backbone further stabilizes the charge distribution, suggesting better charge-transfer capability compared to PCP-PET. Interestingly, in the PCP-TiO_2-PET/PU composite, the red regions are much more dominant, showing a significant increase in electron density across the molecular surface. This highlights the successful integration of TiO_2 and PU, which introduces oxygen-rich domains and polar functional groups. The enhanced electron density is expected to facilitate stronger adsorption of cationic species and promote interfacial charge transfer, a property crucial for photocatalysis and pollutant degradation (Farokhi et al., 2022; Suresh et al., 2022).

3.3 Visual studies:

3.3.1 Quantum Theory of Atoms in Molecules

To gain deeper insight into the nature and strength of the interactions as well as the mechanisms between PCP and the microplastic systems, QTAIM analyses were performed. QTAIM plots revealed clear bond critical points (BCPs) and bond paths between PCP and the polymeric substrates, confirming the formation of noncovalent interaction networks (Kowalik et al., 2021;

Liu et al., 2025). For the PCP-PET, PCP-PU, and PCP-TiO_2-PET/PU systems, the electron density at the BCPs was relatively low ($\varrho^{(r)} < 0.02$ a.u.) with positive Laplacian values ($\nabla^2\varrho^{(r)} > 0$), suggesting that the interactions are primarily closed-shell in nature, dominated by weak van der Waals and electrostatic forces (Bakheit et al., 2023). For the PCP-PET system, bond critical points such as O···H ($\varrho^{(r)} = 0.008$ a.u., $\nabla^2\varrho^{(r)} = 0.037$ a.u.) and O–H···π type interactions indicate weak hydrogen bonding. The positive Laplacian ($\nabla^2\varrho^{(r)} > 0$) with small electron density values confirms closed-shell interactions, dominated by van der Waals and electrostatic forces. ELF values around 0.020-0.030 further support weak non-covalent stabilization (Gobak et al., 2025; Anbukarasi et al., 2023). In the PCP-PU system, multiple O···H hydrogen bonds ($\varrho^{(r)} = 0.007$–0.011 a.u.) with negative total energy density ($H^{(r)} < 0$) indicate slightly stronger stabilization compared to PET. The ratio $G_{(r)}/V_{(r)}$ values falling between –1.3 and –2.0 classify these interactions as partially covalent hydrogen bonds, suggesting a higher adsorption stability. Additionally, Cl···C and Cl···N interactions were detected ($\varrho^{(r)} = 0.005$–0.006 a.u.), highlighting the role of halogen bonding in stabilizing PCP on the PU matrix.

Looking at the QTAIM plot in Figure 4, we observe that PCP-TiO_2-PET–PU nanocomposite exhibited a more complex topology with multiple BCPs forming between PCP and both the polymeric framework and the TiO_2 cluster. The PCP-TiO_2-PET-PU composite exhibited the strongest binding characteristics. Notably, the O···H bond at CP 125 showed $\varrho^{(r)} = 0.045$ a.u. and $\nabla^2\varrho^{(r)} = 0.162$ a.u, with $V_{(r)} = -0.043$ a.u. and $H(r) \approx -0.001$ a.u, confirming the presence of a moderately strong hydrogen bond with partial covalent character. This bond is significantly stronger than those in PET and PU, consistent with the enhanced adsorption energy (–2.594 eV). Moreso, the appearance of multiple O···H contacts with higher density values, together with ELF > 0.1, indicates multi-centered cooperative hydrogen bonding, which drives the strong stabilization of PCP on the TiO_2-modified surface (Liu et al., 2025; Bakheit et al., 2023; Gobak et al., 2025; Anbukarasi et al., 2023).

3.3.2 Non-Covalent Interaction (NCI) Analysis

Complementary, we examined non-covalent interactions in this study, using NCI isosurface plots to visualize the weak forces that govern the stability and adsorption efficiency of the studied complexes (Figure 5). According to reported literature, the color scheme differentiates interaction types: green regions correspond to weak van der Waals (vdW) interactions, blue indicates strong attractive hydrogen bonding, while red reflects steric repulsion (Lu & Chen, 2024). For the PCP-PET system, the NCI plot reveals extensive green patches distributed around the interface of the two fragments, signifying dominant vdW stabilization. A few localized red patches near the hydroxyl and carbonyl groups suggest weak hydrogen bonds powered by steric interactions common among the rings of the different systems (Mahadevi & Sastry, 2016). In the PCP-PU system, the interaction pattern is more pronounced between the chlorophenol and the carbonyl and cyanide groups, indicating vdW stabilization. The presence of nitrogen atoms in PU also promotes more directional non-covalent contacts, consistent with enhanced stabilization compared to PCP-PET.

The reduced density gradient isosurfaces for PCP-PET and PCP-PU were predominantly green, reflecting weak dispersive contacts (Lu & Chen, 2024). In the TiO_2-doped system, however, blue regions appeared around the PCP binding sites, indicating stronger attractive interactions facilitated by TiO_2 incorporation, particularly around the TiO_2–oxygen–hydrogen interaction zones (Wang et al., 2021). As depicted in Figure 5, the PCP-TiO_2-PET–PU system exhibits the richest non-covalent interaction profile. This result highlights the cooperative effect of TiO_2 in enhancing orbital overlap and stabilizing charge transfer interactions between PCP and the host matrix.

3.4 Adsorption studies of PCP

According to reports (Kroes, 2021; Thomas et al., 2023; Saeed & Fischer, 2025), the adsorption energy analysis is a very crucial matrix in validating the strength or efficacy of adsorbate molecules to a host surface, and is either physisorption (weak adsorption) or chemisorption (strong adsorption). The adsorption energy (E_{ads}) was calculated to evaluate the binding affinity of PCP on PET, PU, and the TiO_2-PET/PU composite. PET and PU exhibited adsorption energies of -0.629 eV and -0.656 eV, respectively, which correspond to weak interactions consistent with physisorption. These relatively small negative values suggest limited stabilization of PCP on pristine polymer surfaces, in agreement with their large energy gaps and low softness values. In contrast, the TiO_2-PET/PU composite showed a notably higher adsorption energy of −2.594 eV, indicating significantly stronger and more favorable binding. Calculated by employing equation (1), this substantial increase in interaction strength confirms that TiO_2 incorporation enhances the sorption capacity of the composite, likely through improved charge transfer and electronic polarization effects (Farokhi et al., 2022; Wang et al., 2017). The stronger stabilization of the pollutant–adsorbent complex is further supported by the reduced energy gap and the elevated electrophilicity index observed for the composite upon adsorption.

When compared with previous computational adsorption studies, the observed adsorption energy for PCP on TiO_2-PET/PU (-2.594 eV) is considerably higher and more favorable than typical polymer–pollutant interactions, which are often reported in the range of −0.4 to −1.2 eV (Jiang et al., 2024; Monteiro et al., 2024). It is also comparable to or greater than values reported for adsorption of chlorophenols on metalloporphyrin (Lan et al., 2024), modified graphene (Apebende et al., 2024; Ji et al., 2017), graphitic carbon nitride (Ou et al., 2018; Li et al., 2019), metal oxides (Zong et al., 2025; Song et al., 2011), and carbon-based nanocomposites (− 0.44 to −1.24 eV) (Watkins et al., 2017; Cheon et al., 2024). This comparison highlights that TiO_2 functionalization

significantly elevates the performance of the PET/PU matrix, placing the composite among the more effective sorbents for chlorophenol removal.

Overall, the adsorption energy results demonstrate that while pristine PET and PU are weak adsorbents for 2-chlorophenol (PCP), TiO_2 functionalization imparts superior adsorption capability, making the TiO_2-PET/PU nanocomposite a highly promising candidate for environmental remediation applications.

The relationship between the electrophilicity index (ω) and adsorption energy (Eads) provides insight into the adsorption behavior of chlorophenol on the investigated systems. The calculated results indicate that pristine PET and PU exhibit electrophilicity indices of 4.358 eV and 2.149 eV, respectively, whereas the TiO_2-PET-PU composite shows a higher electrophilicity value (5.729 eV), suggesting an enhanced ability of the composite surface to accept electron density during interaction with adsorbate molecules. Upon interaction with chlorophenol, the adsorption energies reveal a clear trend in adsorption strength. The PCP-PET and PCP-PU systems show moderate adsorption energies of -0.629 eV and -0.656 eV, respectively, indicating relatively weak interactions dominated by non-covalent forces. In contrast, the TiO_2-containing composite exhibits a significantly higher electrophilicity index (8.234 eV) together with a substantially more negative adsorption energy (-2.594 eV) for the PCP-TiO_2-PET-PU complex. This trend indicates that the incorporation of TiO_2 enhances the electron-accepting capability of the composite surface and strengthens the interaction with chlorophenol molecules. The increase in electrophilicity facilitates charge transfer between the adsorbent and adsorbate, which is consistent with the stronger adsorption energy predicted for the composite system. These results suggest that the TiO_2-modified PET/PU composite possesses improved adsorption capability compared to the individual polymer components, thus highlighting the role of electronic structure modification and enhanced interaction sites in promoting chlorophenol uptake in aqueous systems.

CONCLUSIONS

In this work, the adsorption behavior of PET/PU-based microplastics modified with TiO_2 toward chlorophenol (PCP) pollutants was systematically investigated through both experimental and theoretical approaches. Structural characterization using FT-IR spectroscopy confirmed the successful incorporation of functional groups relevant to pollutant adsorption. Density Functional Theory (DFT) revealed that TiO_2 modification markedly enhances electronic reactivity as the band gap drops from 5.302 eV for PET and 5.278 eV for PU to 3.160 eV (TiO_2–PET–PU) and further to 2.489 eV upon PCP adsorption. Consistently, adsorption energetics show a step-change from weak physisorption on the pristine polymers (E_{ads} = – 0.629 eV on PET; – 0.656 eV on PU) to strong binding on the composite (E_{ads} = –2.594 eV, ≈ –250 kJ/mol). Interaction-level analyses pinpoint the origin of this gain. NBO gives the largest stabilization in the composite via $LP_{(3)}O_{77} \rightarrow LP^*_{(1)}H_{78}$ donation ($E^{(2)}$ = 392.35 kcal/mol), exceeding the π→π* delocalization seen in PET/PU (≈126 –259 kcal/mol). NCI maps show extended green isosurfaces and localized blue patches around the TiO_2/urethane region, evidencing cooperative H-bonding, π–π/CH···O, and dispersive anchoring unavailable on the pristine polymers. Collectively, our result demonstrates that embedding TiO_2 into a PET/PU microplastic matrix creates a stable, multi-active surface, amplifies electron-acceptor character and charge-transfer capacity, and delivers ~4X stronger PCP adsorption than the unmodified polymers. These further give mechanistic and quantitative insights to convert waste-derived microplastics into high-affinity sorbents for chlorophenols and related petroleum pollutants.

REFERENCES

Adak, B., Butola, B. S., & Joshi, M. (2019). Calcination of UV shielding nanopowder and its effect on weather resistance property of polyurethane nanocomposite films. *Journal of Materials Science*, 54(19), 12698-12712. [Crossref]

Ali, A. M., Rashid, K. T., Yahya, A. A., Majdi, H. S., Salih, I. K., Yusoh, K., ... & Figoli, A. (2021). Fabrication of gum arabic-graphene (Gga) modified polyphenylsulfone (PPSU) mixed matrix membranes: A systematic evaluation study for ultrafiltration (UF) applications. *Membranes*, 11(7), 542. [Crossref]

Ali, A., Chiang, Y. W., & Santos, R. M. (2022). X-ray diffraction techniques for mineral characterization: A review for engineers of the fundamentals, applications, and research directions. *Minerals*, 12(2), 205. [Crossref]

Alkhaldi, H., Alharthi, S., Alharthi, S., AlGhamdi, H. A., AlZahrani, Y. M., Mahmoud, S. A., ... & Abaza, S. F. (2024). Sustainable polymeric adsorbents for adsorption-based water remediation and pathogen deactivation: A review. *RSC Advances*, 14(45), 33143-33190. [Crossref]

Ambrose, A., Rajappan, K., Munuswami Ramanujam, G., & Anilkumar, A. K. (2025). Anti-oxidant and anti-bacterial behavior of sodium alginate patches fortified with polyurethane and Ag-MOF as potential future wound healing material. *Polymer-Plastics Technology and Materials*, 64(2), 238-252. [Crossref]

An, L., Liu, Q., Deng, Y., Wu, W., Gao, Y., & Ling, W. (2020). Sources of microplastic in the environment. In *Microplastics in terrestrial environments: Emerging contaminants and major challenges* (pp. 143-159). Springer International Publishing. [Crossref]

Anbukarasi, K., Xavier, S., Hasan, A. H., Er, Y. L., Jamalis, J., Sebastian, S., & Periandy, S. (2023). DFT and molecular docking analysis of newly synthesized compound (2E)-3-[3-(benzyloxy)phenyl]-1-(4'-chlorophenyl)-2-propen-1-one [BPCLPO]. *Current Physical Chemistry*, 13(1), 37-74. [Crossref]

Apebende, C. G., Amodu, I. O., Ogbogu, M. N., Unimuyi, U. P., Raimi, M. A., & Igomah, G. O. (2024). Computational modelling of

graphene/aluminum nitride (GP/AlN) hybrid materials for the detection of 2,4-dichlorophenoxyacetic acid (DCP) pollutant. *RSC Advances*, 14(30), 21901-21914. [Crossref]

Arif, M., Javed, M., & Akhter, T. (2024). Crosslinked polymeric networks of TiO2-polymer composites: A comprehensive review. *RSC Advances*, 14(46), 33843-33863. [Crossref]

Bakheit, A. H., Al-Salahi, R., Ghabbour, H. A., Ali, E. A., AlRuqi, O. S., & Mostafa, G. A. (2023). Synthesis, X-ray crystal structure, and computational characterization of tetraphenylborate, 3-(5H-dibenzo[a,d]cyclohepten-5-ylidene)-N,N-dimethyl-1-propanamine. *Crystals*, 13(7), 1088. [Crossref]

Becke, A. D. (1993). Density-functional thermochemistry. III. The role of exact exchange. *The Journal of Chemical Physics*, 98(7), 5648-5652. [Crossref]

Beigh, S. (2024). A phytochemicals approach towards the role of dioxins in disease progression targeting various pathways: Insights. *Indian Journal of Pharmaceutical Education and Research*, 58(3s), s732-s756. [Crossref]

Bytautas, L., Klein, D. J., Tzeli, D., Ferrer, M., Elguero, J., Alkorta, I., & Oliva-Enrich, J. M. (2022). Progress in electronic-structure based computational methods: From small molecules to large molecular systems of biological significance. *Frontiers in Computational Chemistry: Volume 6*, 235-284. [Crossref]

Cao, Y., Malekshah, R. E., Heidari, Z., Pelalak, R., Marjani, A., & Shirazian, S. (2021). Molecular dynamic simulations and quantum chemical calculations of adsorption process using amino-functionalized silica. *Journal of Molecular Liquids*, 330, 115544. [Crossref]

Cheon, S., Zhu, S., Gao, Y., Li, J., Harmon, N. J., Zhang, W., ... & Wang, H. (2024). Neighboring catalytic sites are essential for electrochemical dechlorination of 2-chlorophenol. *Journal of the American Chemical Society*, 146(36), 25151-25157. [Crossref]

Combrzyński, M., Oniszczuk, T., Kupryaniuk, K., Wójtowicz, A., Mitrus, M., Milanowski, M., ... & Matwijczuk, A. (2021). Physical properties, spectroscopic, microscopic, X-ray, and chemometric analysis of starch films enriched with selected functional additives. *Materials*, 14(10), 2673. [Crossref]

Costa, T. B., Santana, G. B., Silva, E. M., Conceição, K. G., Diaz, G. Z., Melo, D. Q., ... & Vidal, C. B. (2024). Impact of UV-B photoaging on chlorpyrifos adsorption by PET microplastics: Insights from experimental and DFT analysis. *ACS Omega*, 9(46), 46439-46446. [Crossref]

Cova, T. F., Murtinho, D., Garcia, R., Pais, A. A., & Valente, A. J. (2021). Cyclodextrin-based polymers for pollutant removal. In *Applications of biodegradable and bio-based polymers for human health and a cleaner environment* (pp. 335-438). Apple Academic Press. [Crossref]

Das, K. P., Chauhan, P., Staudinger, U., & Satapathy, B. K. (2024). Exploring sustainable adsorbents to mitigate micro-/nano-plastic contamination: Perspectives on electrospun fibrous constructs, biochar, and aerogels. *Environmental Science: Advances*. [Crossref]

Dong, L., Xie, P., Zhang, X., Qiao, J., Rao, D., Sun, Y., & Guan, X. (2022). Co-present Pb(II) accelerates the oxidation of organic contaminants by permanganate: Role of Pb(III). *Frontiers of Environmental Science & Engineering*, 16(8), 109. [Crossref]

Enyoh, C. E., & Wang, Q. (2024). Combined experimental and molecular dynamics removal processes of contaminant phenol from simulated wastewater by polyethylene terephthalate microplastics. *Environmental Technology*, 45(6), 1183-1202. [Crossref]

Fan, W., Gualtieri, A. F., Hamilton, A., Patel, J. P., & Salmond, J. A. (2025). Determining factors affecting the accuracy of SEM-EDX data-based quantitative chemical analysis for identifying naturally occurring individual carcinogenic erionite fibers. *Scientific Reports*, 15(1), 25316. [Crossref]

Farokhi, A., Shahroosvand, H., Delle Monache, G., Pilkington, M., & Nazeeruddin, M. K. (2022). The evolution of triphenylamine hole transport materials for efficient perovskite solar cells. *Chemical Society Reviews*, 51(14), 5974-6064. [Crossref]

Frescura, L. M., de Menezes, B. B., Junior, R. A. F., Mortari, S. R., de Moraes Bastos, A. F., & da Rosa, M. B. (2024). Polycyclic aromatic hydrocarbon derivatives onto polar microplastics of polyurethane: Equilibrium, thermodynamics, and kinetics of monolayer-multilayer adsorption. *Environmental Science and Pollution Research*, 31(43), 55158-55168. [Crossref]

Frisch, M. J., Trucks, G. W., Schlegel, H. B., Scuseria, G. E., Robb, M. A., Cheeseman, J. R., ... & Fox, D. J. (2016). *Gaussian 16*. Gaussian, Inc.

Gobak, K. H., A, S. A., Runde, M., Qadir, K. W., & Abubakar, M. N. (2025). A computational study of organosulfur adsorption on silicon fullerenes: Implications for improving environmental safety. *Silicon*, 1-14. [Crossref]

Goodfellow, A. S., & Bühl, M. (2021). Hydricity of 3d transition metal complexes from density functional theory: A benchmarking study. *Molecules*, 26(13), 4072. [Crossref]

Guan, H., Sun, H., & Zhao, X. (2025). Application of density functional theory to molecular engineering of pharmaceutical formulations. *International Journal of Molecular Sciences*, 26(7), 3262. [Crossref]

Haritha, M., & Suresh, C. H. (2024). Unveiling drug discovery insights through molecular electrostatic potential analysis. *Wiley Interdisciplinary Reviews: Computational Molecular Science*, 14(6), e1735. [Crossref]

Huang, Y., Rong, C., Zhang, R., & Liu, S. (2017). Evaluating frontier orbital energy and HOMO/LUMO gap with descriptors from density functional reactivity theory. *Journal of Molecular Modeling*, 23(1), 3. [Crossref]

Humphrey, W., Dalke, A., & Schulten, K. (1996). VMD: Visual molecular dynamics. *Journal of Molecular Graphics*, 14(1), 33-38. [Crossref]

Ji, M., Cheng, X., & Wu, W. (2017). Al-doped graphene as an effective adsorber for some toxic derivatives of aromatic hydrocarbons. *Journal of Theoretical and Computational Chemistry*, 16(1), 1750004. [Crossref]

Jiang, H., & Hu, H. (2024). Sustainable synergistic adsorption of tetracycline in water by biochar and microplastics: Exploration of the mechanism of DFT. *Journal of Water Process Engineering*, 66, 105998. [Crossref]

Jiang, H., Ding, Z., Lei, X., Li, X., Que, S., Zhou, J., ... & Sun, D. (2024). Competitive adsorption studies of Cd(II) and As(III) by poly(butylene succinate) microplastics: Based on experimental and theoretical calculation. *Water*, 17(1), 74. [Crossref]

Jiang, Z., Huang, L., Fan, Y., Zhou, S., & Zou, X. (2022). Contrasting effects of microplastic aging upon the adsorption of sulfonamides and its mechanism. *Chemical Engineering Journal*, 430, 132939. [Crossref]

Ketegenov, T., Kamunur, K., Batkal, A., Gani, D., & Nadirov, R. (2022). Recent advances in the preparation of barium sulfate nanoparticles: A mini-review. *ChemEngineering*, 6(2), 30. [Crossref]

Khachay, A., Yous, R., Khalladi, R., Cherifi, H., Belaid, B., Alharthi, M. N., ... & Mouni, L. (2025). Understanding the adsorption mechanism of phenol and para-chlorophenol onto sepiolite clay: A combined DFT calculations, molecular dynamics simulations, and isotherm analysis. *Water*, 17(9), 1335. [Crossref]

Kowalik, M., Brzeski, J., Gawrońska, M., Kazimierczuk, K., & Makowski, M. (2021). Experimental and theoretical investigation of conformational states and noncovalent interactions in crystalline sulfonamides with a methoxyphenyl moiety. *CrystEngComm*, 23(35), 6137-6162. [Crossref]

Kroes, G. J. (2021). Computational approaches to dissociative chemisorption on metals: Towards chemical accuracy. *Physical Chemistry Chemical Physics*, 23(15), 8962-9048. [Crossref]

Kumar, R., Kumar, M., Kumar, A., Singh, R., Kashyap, R., Rani, S., & Kumar, D. (2019). Surface modification of graphene oxide using esterification. *Materials Today: Proceedings*, 18, 1556-1561. [Crossref]

Lan, W., Meng, Y., Kong, X., Wang, X., & Nie, C. (2024). Exploring the activation potential of heme for 2,4-dichlorophenol, 2,4,6-trichlorophenol, and pentachlorophenol. *Scientific Reports*, 14(1), 23212. [Crossref]

Lazić, V., & Nedeljković, J. M. (2024). Photocatalytic reactions over TiO2-based interfacial charge transfer complexes. *Catalysts*, 14(11), 810. [Crossref]

Li, Z., Meng, X., & Zhang, Z. (2019). Fabrication of surface hydroxyl modified g-C3N4 with enhanced photocatalytic oxidation activity. *Catalysis Science & Technology*, 9(15), 3979-3993. [Crossref]

Liu, F. F., Wang, S. C., Zhu, Z. L., & Liu, G. Z. (2021). Current progress on marine microplastics pollution research: A review on pollution occurrence, detection, and environmental effects. *Water*, 13(12), 1713. [Crossref]

Liu, X. M., Zhao, D. X., & Yang, Z. Z. (2025). Transition from noncovalent interaction to covalent bond based on one-electron potential, quantum chemical topology, and molecular face theory. *The Journal of Physical Chemistry A*. [Crossref]

Liu, Z., Qin, Q., Hu, Z., Yan, L., Ieong, U. I., & Xu, Y. (2020). Adsorption of chlorophenols on polyethylene terephthalate microplastics from aqueous environments: Kinetics, mechanisms and influencing factors. *Environmental Pollution*, 265, 114926. [Crossref]

Lu, T., & Chen, F. (2012). Multiwfn: A multifunctional wavefunction analyzer. *Journal of Computational Chemistry*, 33(5), 580-592. [Crossref]

Lu, T., & Chen, Q. (2024). Visualization analysis of weak interactions in chemical systems. *Comprehensive Computational Chemistry*, 2, 240-264. [Crossref]

Mahadevi, A. S., & Sastry, G. N. (2016). Cooperativity in noncovalent interactions. *Chemical Reviews*, 116(5), 2775-2825. [Crossref]

Markandan, M., Sepperumal, U., & Rodríguez, L. V. C. (2020). Bacterial (*Alcaligenes faecalis*) degradation of PET (poly(ethylene terephthalate)) obtained from old bottles wastes. *Acta Microbiologica Bulgarica*, 36, 145.

Mathew, N., Somanathan, A., Tirpude, A., Pillai, A. M., Mondal, P., & Arfin, T. (2025). Dioxins and their impact: A review of toxicity, persistence, and novel remediation strategies. *Analytical Methods*. [Crossref]

Mecozzi, M., & Nisini, L. (2019). The differentiation of biodegradable and non-biodegradable polyethylene terephthalate (PET) samples by FTIR spectroscopy: A potential support for the structural differentiation of PET in environmental analysis. *Infrared Physics & Technology*, 101, 119-126. [Crossref]

Mohamed, M. A., Jaafar, J., Ismail, A. F., Othman, M. H. D., & Rahman, M. A. (2017). Fourier transform infrared (FTIR) spectroscopy. In *Membrane characterization* (pp. 3-29). Elsevier. [Crossref]

Montazeri, N., Salahshoori, I., Feyzishendi, P., Miri, F. S., Mohseni, M. M., & Khonakdar, H. A. (2023). pH-sensitive adsorption of gastrointestinal drugs (famotidine and pantoprazole) as pharmaceutical pollutants by using the Au-doped@ZIF-90-glycerol adsorbent: Insights from computational modeling. *Journal of Materials Chemistry A*, 11(47), 26127-26151. [Crossref]

Monteiro, N. D. K. V., Bezerra, L. L., & Machado, R. J. D. A. (2024). Modeling the adsorption mechanism of 3-tertiary-butyl-4-hydroxyanisole (3BHA) on polyethylene and polypropylene microplastics. *Chemical Papers*, 78(4), 2359-2367. [Crossref]

Mou, Z., Chen, X., Du, Y., Wang, X., Yang, P., & Wang, S. (2011). Forming mechanism of nitrogen doped graphene prepared by thermal solid-state reaction of graphite oxide and urea. *Applied Surface Science*, 258(5), 1704-1710. [Crossref]

Ou, H., Zhang, W., Yang, X., Cheng, Q., Liao, G., Xia, H., & Wang, D. (2018). One-pot synthesis of g-C3N4-doped amine-rich porous organic polymer for chlorophenol removal. *Environmental Science: Nano*, 5(1), 169-182. [Crossref]

Park, Y. (2024). *Altering framework topology and heteroatom distributions of molecular sieves by designed organic structure-directing agents* [Doctoral dissertation, California Institute of Technology]. [Crossref]

Saeed, L., & Fischer, M. (2025). Mechanistic insights into 5-fluorouracil adsorption on clinoptilolite surfaces: Optimizing DFT parameters for natural zeolites, Part II. *Applied Sciences*, 15(17), 9535. [Crossref]

Semenov, S. G., Bedrina, M. E., & Klemeshev, V. A. (2023). Electronic state of arsenic endo-atom and indices of interatomic bonds in [As@Ni12As20]3-/0, As20, Ni12As20, As@C60, and As@C70 clusters. *Russian Journal of General Chemistry*, 93(2), 369-374. [Crossref]

Semidalas, E., & Martin, J. M. (2020). Canonical and DLPNO-based G4(MP2)XK-inspired composite wave function methods parametrized against large and chemically diverse training sets: Are they more accurate and/or robust than double-hybrid DFT? *Journal of Chemical Theory and Computation*, 16(7), 4238-4255. [Crossref]

Shi, Y., Zheng, L., Huang, H., Tian, Y. C., Gong, Z., Liu, P., ... & Gao, S. (2023). Formation of nano- and microplastics and dissolved chemicals during photodegradation of polyester base fabrics with polyurethane coating. *Environmental Science & Technology*, 57(5), 1894-1906. [Crossref]

Shoukat, A., Zubair, M., Uddin, J., Khan, A., & Al-Harrasi, A. (2023). Innovative synthesis of non-porous polyurethane membranes with enhanced mechanical, thermal and adsorption properties. *Polymer Bulletin*, 80(7), 7429-7450. [Crossref]

Shrestha, S. (2016). Chemical, structural and elemental characterization of biosorbents using FE-SEM, SEM-EDX, XRD/XRPD and ATR-FTIR techniques. *Journal of Chemical Engineering and Process Technology*, 7(3), 1-11. [Crossref]

Sidra, Khan, M. H., Quan, W. J., Ahmad, S., Ji, J., Xiao, X., ... & Ali, N. (2024). Bio-graphene foam: A robust solution for adsorptive and sustainable chlorophenol removal from wastewater. *Water, Air, & Soil Pollution*, 235(12), 766. [Crossref]

Song, K., Zhang, D., & Liu, C. (2011). DFT study of the interactions of 2-chlorophenol/2-chlorophenoxy radical with the (6,0) single-walled ZnO nanotubes with and without an oxygen vacancy. *Computational and Theoretical Chemistry*, 978(1-3), 98-103. [Crossref]

Suresh, C. H., Remya, G. S., & Anjalikrishna, P. K. (2022). Molecular electrostatic potential analysis: A powerful tool to interpret and predict chemical reactivity. *Wiley Interdisciplinary Reviews: Computational Molecular Science*, 12(5), e1601. [Crossref]

Suresh, C., & Haritha, M. (2024). Unveiling drug discovery insights through molecular electrostatic potential analysis. *ChemRxiv*. [Crossref]

Thomas, S., Mayr, F., Madam, A. K., & Gagliardi, A. (2023). Machine learning and DFT investigation of CO, CO2 and CH4 adsorption on pristine and defective two-dimensional magnesene. *Physical Chemistry Chemical Physics*, 25(18), 13170-13182. [Crossref]

VL, D. S., Rajmohan, G., Nagasubramanian, K., & Venkatachalam, P. (2025). Improving the binding affinity of plastic degrading cutinase with polyethylene terephthalate (PET) and polyurethane (PU); An in-silico study. *Heliyon*, 11(2). [Crossref]

Wang, B., Bozal-Ginesta, C., Zhang, R., Zhou, B., Ma, H., Jiao, L., ... & Li, Z. (2021). A supramolecular H12SubPcB-OPhCOPh/TiO2 Z-scheme hybrid assembled via dimeric concave-ligand π-interaction for visible photocatalytic oxidation of tetracycline. *Applied Catalysis B: Environmental*, 298, 120550. [Crossref]

Wang, N., Feng, J., Chen, J., Wang, J., & Yan, W. (2017). Adsorption mechanism of phosphate by polyaniline/TiO2 composite from wastewater. *Chemical Engineering Journal*, 316, 33-40. [Crossref]

Watkins, M., Sizochenko, N., Moore, Q., Golebiowski, M., Leszczynska, D., & Leszczynski, J. (2017). Chlorophenol sorption on multi-walled carbon nanotubes: DFT modeling and structure–property relationship analysis. *Journal of Molecular Modeling*, 23(2), 39. [Crossref]

Wei, D., Zhao, C., Khan, A., Sun, L., Ji, Y., Ai, Y., & Wang, X. (2019). Sorption mechanism and dynamic behavior of graphene oxide as an effective adsorbent for the removal of chlorophenol based environmental-hormones: A DFT and MD simulation study. *Chemical Engineering Journal*, 375, 121964. [Crossref]

Weinhold, F. (2012). Natural bond orbital analysis: A critical overview of relationships to alternative bonding perspectives. *Journal of Computational Chemistry*, 33(30), 2363-2379. [Crossref]

Wu, S., Li, X., Tian, Y., Lin, Y., & Hu, Y. H. (2021). Excellent photocatalytic degradation of tetracycline over black anatase-TiO2 under visible light. *Chemical Engineering Journal*, 406, 126747. [Crossref]

Yi, P., Hu, H., Sui, W., Zhang, H., Lin, Y., & Li, G. (2020). Thermoresponsive polyurethane sponges with temperature-controlled superwettability for oil/water separation. *ACS Applied Polymer Materials*, 2(5), 1764-1772. [Crossref]

Yusuf, M. O. (2023). Bond characterization in cementitious material binders using Fourier-transform infrared spectroscopy. *Applied Sciences*, 13(5), 3353. [Crossref]

Zhang, Q., Chen, J., Gao, X., Che, H., Ao, Y., & Wang, P. (2022b). Understanding the mechanism of interfacial interaction enhancing photodegradation rate of pollutants at molecular level: Intermolecular π-π interactions favor electrons delivery. *Journal of Hazardous Materials*, 430, 128386. [Crossref]

Zhang, Q., Chen, J., Gao, X., Che, H., Wang, P., Liu, B., & Ao, Y. (2022a). Enhanced photocatalytic degradation of bisphenol A by a novel donor-acceptor g-C3N4: π-π interactions boosting the adsorption and electron transfer behaviors. *Separation and Purification Technology*, 300, 121947. [Crossref]

Zhao, G., & Zhu, H. (2020). Cation-π interactions in graphene-containing systems for water treatment and beyond. *Advanced Materials*, 32(22), 1905756. [Crossref]

Zhao, G., Li, W., Xu, C., Qin, Q., Fan, W., Li, X., & Zhao, D. (2024). Adsorption mechanism of cefradine on three microplastics: A combined molecular dynamics simulation and density functional theory calculation study. *Science of the Total Environment*, 951, 175690. [Crossref]

Zhurko, G. A., & Zhurko, D. A. (2005). *Chemcraft – Graphical program for visualization of quantum chemistry computations* (Academic version 1).

Zong, Z., Wang, C., Zhao, M., Chen, W., & Jia, Y. (2025). Adsorption and dissociation of 2-chlorophenols on the 2D ZnO monolayer decorated with Al atoms: A DFT study. *Materials*, 18(4), 813. [Crossref]